Shocked soil - a rare terrestrial impactite

Shawn P. Wright and Joseph R. Michalski

Department of Earth Sciences and the Laboratory for Space Research, the University of Hong Kong, Hong Kong

James Lee Building, University of Hong Kong, Pokfulam Road, Hong Kong

Corresponding author: Shawn Wright (swright@hku.hk)

Abstract

Impactites generally consist of target rocks subjected to a shock wave during an impact event, but theoretically can be composed of surficial materials such as soil or other unconsolidated surface materials. Frothy samples found in the impact melt-bearing breccia circum Lonar crater, India have a significantly lower density than shocked bedrock basalts. Analyses of petrographic and back-scattered electron images, along with mineralogical and geochemical comparisons between the target basalts and local Deccan soils suggest that these are shocked soils that were compressed and lithified during the impact event. Hyperspectral images reveal both unshocked and shocked silicates and glasses along with organics on a scale of millimeters. Shocked soils/regolith could hold tremendous value as recorders of ancient lithosphere-hydrosphere-atmosphere reactions on this planet as well as Mars.

Plain Language Summary

A fresh ejecta blanket of an impact crater contains two layers: an underlying lithic breccia and an overlying, thinner breccia with clasts of glasses of shock-metamorphosed materials. These shocked clasts generally have a protolith/precursor that are bedrock lithologies of the target rock sequence. However, rare clasts in the suevite breccia have been identified that used to be paleosol ("old soil") in the Deccan region surrounding what is now Lonar crater, India. We compared the minerals, whole rock geochemistry of major elements, and microscopic texture of these glassy clasts to shocked basalts, unshocked Deccan basalt, and local soil samples. Comparisons to previously-published data were also performed. Shocked soils likely exist at other terrestrial impact sites; however surficial materials at the most common terrestrial impact crater targets – felsic granites or metagranites and clastic sedimentary rocks – resemble the

mineralogy and texture of the local bedrock. Thus a shocked soil would be difficult to recognize at these locations. Mafic basalt, however, alters to clays at much higher rates and to finer soil grain sizes. While rare on Earth, basaltic shocked soils might be more widespread on Mars and candidates for sample return or up-close rover investigations.

Introduction and Background

Impactites are the products of impact cratering. A large majority of impactites are rocks that have been fractured and transported at relatively low shock pressures during the impact process. A smaller amount of impactites have experienced higher shock pressures that result in mineralogical changes and transformations to impact melts and other impact glasses such as diaplectic glasses and partial melts (all 19 chapters of Osinski and Pierazzo 2013, including Newsom et al. 2013). Lonar crater in Maharashtra, India is a ~1.8-km-diameter impact crater with a wide range of well-preserved impactites (Kieffer et al. 1976) of tremendous geological value for understanding fundamental impact processes on this planet or other planets containing basaltic target rocks.

As the majority of the target sequence at Lonar crater, India was bedrock Deccan basalt, clasts of these dense volcanic rocks are found in two ejecta layers (as breccias). In addition, ground-hugging ejecta flows have incorporated surface materials (such as soils) as rip-up clasts incorporated into the lower lithic ejecta layer (Maloof et al. 2010; Stewart et al. 2005). Shoemaker (1960) described the emplacement of these two breccias at Meteor Crater as the upper “fall out” ejecta unit overlying the lower, thicker “throw out” ejecta unit. Here, we

introduce the findings of a surficial material, pre-impact soil, that was shocked to a glass and deposited as clasts into the upper "suevite" breccia unit (aka impact melt-bearing breccia).

The soil in the Deccan region (Nagelschmidt et al. 1940; Bhattacharyya et al. 1993; Widdowson et al. 1997; Salil et al. 1997; Ghosh et al. 2006; Sayyed and Hundekari 2006; Pal et al. 2013) has a basaltic geochemistry (Nesbit and Young 1989; Nesbit and Wilson 1992; Babechuk et al. 2014) with occurrences of smectite and growths of heulandite, other zeolites, hematite, silica, and carbonates. The black clay-rich soil found on the Deccan basalt flows is noted by several previous field workers at Lonar crater (Fudali et al. 1980; Maloof et al. 2010) as being an ideal marker bed because it dates to the time just prior to/at impact and it clearly underlies the lithic ejecta unit (Stewart et al. 2005). As the lithic ejecta layer was emplaced during the impact event 576 ± 47 ka (Jourdan et al. 2011; Schmieder and Kring 2020), it covered and incorporated some of this pre-impact paleosol, as clumps of soil are found as cm-sized clasts throughout the lower lithic breccia (Fudali et al. 1980; Stewart et al. 2005). In this paper, we investigate this same paleosol being shocked and emplaced as the smallest clasts in the overlying impact melt-bearing "suevite" breccia unit at Lonar crater.

Sample collection and preliminary petrography

Fieldwork in the Lonar ejecta blanket over several field seasons (*e.g.,* Wright et al. 2011; Newsom et al. 2013) in 2010, 2016, and 2018 yielded a collection of frothy, low-density samples unlike traditional shocked basalt in which bedrock basalt was the protolith (Kieffer et al. 1976) (Figure 1, supplemental figure S1). All of these samples shown (Figure 1) and discussed in this paper are clasts from the suevite breccia or impact melt-bearing breccia (Shoemaker 1960,

Kieffer et al. 1976). These clasts were pulled directly from the breccia in the eastern ejecta blanket. Supplemental figure S1 describes the location and ejecta characteristics of the suevite or impact melt-bearing breccia in the eastern ejecta blanket. Note that at times, the very fine suevite matrix adheres to some breccia clasts, but these fines are not the topic of this paper. One unique sample clast in the suevite breccia was found to be a contact of a shocked bedrock basalt with diaplectic labradorite glass and the unique material described here; a cut slice of this clast and the contact between the two are shown in Figure 1. Other, smaller samples shown in Figure 1 were found as clasts amidst other clasts from a range of shock pressures resulting in both maskelynite-bearing shocked basalts (Class 2 or shock stage M-S4) through impact melts (Class 5 classified by Kieffer et al. 1976) or shock stage M-S7 (Stöffler et al. 2018)). Petrographic images of three polished thin sections revealed a texture unlike that of Deccan basalt or any target bedrock at Lonar crater as shown in petrographic images in Kieffer et al. (1976), Wright et al. (2011), and supplemental figure S2 accompanying this paper. The apparent mineralogy of these samples (from our petrographic observations) matches mineralogies described for Deccan soils (Nagelschmidt et al. 1940; Bhattacharyya et al. 1993; Widdowson et al. 1997; Salil et al. 1997; Ghosh et al. 2006; Sayyed and Hundekari 2006; Pal et al. 2013), but with melt glass and maskelynite needles in addition to the secondary minerals listed above and described in these references. Back-scattered electron (BSE) images of two of the shocked samples and a paleosol were taken for more insight into the sample texture and composition, and other means described below were used to understand the mineralogy and texture at a higher scale. The analyses used for the three shocked soils and three paleosols are shown as Supplemental Figure S3.

Methods

Thin sections of two purported shocked soils and one thin section of a definitive pre-impact soil were examined on the JEOL JXA-8530F electron probe at Johnson Space Center. A pre-impact soil sample LC15-PS-460 (supplemental figure S3) was collected under the distal lithic ejecta in the western ejecta blanket at ~ 2.1 crater radii from crater center (Stewart et al. 2005; Maloof et al. 2010). The XRF geochemistry of this sample and a second paleosol collected from under the Lonar ejecta were averaged with previously-published geochemistries of Lonar paleosol (Ray et al. 2017) to produce an average of Lonar paleosols for comparisons to both bedrock basalt and the shocked soil.

X-ray diffraction (XRD) data were acquired for six samples: two paleosols, two shocked soils, an unshocked Deccan/Lonar basalt, and a shocked Lonar basalt. X-ray data were collected from random powder mounts over 2° to 80° 2-theta in 0.1° steps using cobalt radiation on a Rigaku MiniFlex instrument in the Planetary Spectroscopy and Mineralogy Laboratory at the University of Hong Kong. Data processing and mineral identification were carried out using JADE software and the MDI 500 mineral library. This reference library contains sufficient minerals for most geological applications, but we note that no widely available reference library contains a wide range of poorly crystalline materials.

Samples of three shocked soils and two paleosols were finely powdered and sent to the Franklin and Marshall XRF Lab to measure the abundance of major, minor, and trace elements in the samples with X-ray fluorescence (XRF). Five to ten grams of material was necessary for minor and trace element geochemistry. Powders were heated until molten, and then quenched into a glass disk. After standards are analyzed for each major element, 30 to 50 data points are acquired for each element, with the results presented as percent oxides. The goal was to examine if the geochemistry of soil differed from Deccan and Lonar basalt. Whereas wholly similar,

there are very slight geochemical differences between basalt in the Lonar region (from the Poladpur Formation of the Wai sub-group of the Deccan) and other members of Deccan basalt (Vanderkluysen et al. 2011; Babechuk et al. 2014; Suhr et al. 2018). Soils, however, should be dissimilar from bedrock basalt (Nesbit and Wilson 1992; Babechuk et al. 2014). We use an average of 19 bedrock basalt samples from the Lonar region from Osae et al. (2005) that Ray et al. (2017) suggest be used as an "average Lonar basalt" geochemistry, and use another five fresh Lonar basalt geochemistries from Peng et al. (2014) for additional comparisons between basalt, paleosol, and shocked soils.

We examined thin sections of the three shocked soils on a Nicolet Continuum FT-IR microscope in the Planetary Spectroscopy and Mineralogy Laboratory at the University of Hong Kong. Calibrated hyperspectral reflectance images were collected using a gold reference standard from ~650 to 4000 cm^{-1} at 4 cm^{-1} spectral resolution. The spectral spot size was ~30 μm collected systematically over the field of views. This work is focused on interpretation of spectra from 700-2000 cm^{-1} in order to identify minerals and amorphous phases from fundamental vibrations (*e.g*. Si-O, C-O). Data reduction and compositional mapping were carried out using principal component analysis (PCA).

Results

Petrography and High Resolution Images

The petrography of two shocked soils are shown in Figure 2 (A through F) and compared to one of the unshocked paleosols (Figure 2GH). Whereas unshocked paleosol shows comminuted

pieces of labradorite and augite (from basalt) within opaque organics and calcite/caliche, the shocked soils show schlieren of "flowing" calcite evident as high birefringence regions under cross polarized light (Figures 2CDEF). This calcite can also be seen on the hand samples (Figure 1). The shocked soils contain augite and labradorite, but these are now 5-10 μm comminuted particles (labelled in Figure 3B and 3D) and no longer their original state as larger euhedral crystals seen in unshocked and shocked basalts from Lonar crater (supplemental figure S2, Kieffer et al. 1976; Wright et al. 2011). These specks of augite and labradorite are surrounded by organics and clays best seen in the PPL images (Figures 3A and 3C).

The petrography of one shocked soil sample (LC09-316) showed many more remnants or relics of unshocked soil clumps within the glass than the other two shocked soils. Thus, we obtained photomicrographs with a higher magnification (20X to 40X) on the petrographic microscope to reveal their texture with this sample (Figure 3). Figure 3 shows these remnants still have the original desiccation cracks seen in terrestrial soils such as the petrography of the unshocked soil sample seen in Figure 2GH. Figure 3E shows nearly the same field of view as the BSE image in Figure 4A and a contextual petrographic image of this region is shown as supplemental figure S5.

Where compared to BSE images of shocked basalt (Wright et al. 2011; Newsom et al. 2013), BSE images of the shocked soils show melted labradorites and melted augites from a full range of shock pressures (Stoffler et al., 2018) (Figure 4). This particular BSE image (Figure 4A) was selected to display a typical BSE image texture of the shocked soils but with a region of unmelted, unshocked soil protolith within the shocked soil. On the right of the BSE image are the same small, irregular fragments of augite, oxides, labradorites, and maskelynites that can be seen on the right sides of petrographic images in Figures 2AB and 2CD, and throughout 2EF, but

at a higher resolution and scale. On the left are dark organics, clays and frothy calcite with three labradorites or maskelynite regions at the top. This texture is different from the texture of bedrock Deccan basalt (Kieffer et al. 1976; Wright et al. 2011). The Figure 4 caption discusses the findings of regions of unshocked soil with pre-shock dessication features within the shocked glasses. A "halo" of melt texture around the unshocked soil remnants best seen in Figures 4C and 4D suggest that the protolith of the melt around the remnants was also soil.

Mineralogy

A comparison of the six XRD patterns (Figure 4) shows several key features of shocked and unshocked soils and rocks. The two most important aspects of the XRD patterns of the shocked materials (Figure 4A) is that they have wider diffraction peaks (larger FWHM) in general and a broad background of amorphous material located from ~20° to 40° 2-theta. This is true of the shocked soils and shocked maskelynite-bearing bedrock basalt (Figure 4C), and suggests a decrease in crystallinity as compared to the XRD patterns of unshocked materials in Figure 4B and 4C.

The mineralogies of all four soils agree with previous minerals described for Deccan soils (Nagelschmidt et al. 1940; Bhattacharyya et al. 1993; Widdowson et al. 1997; Salil et al. 1997; Ghosh et al. 2006; Sayyed and Hundekari 2006; Pal et al,. 2013). XRD results of the unshocked paleosols show three major components (smectite, plagioclase and quartz), and several minor components (augite, hematite and calcite). The shocked soils contain similar evidence for plagioclase, quartz, augite and hematite components, but the shocked samples contain much less smectite. Experimental results show that clays could be converted to amorphous materials at shock pressures of 30 – 40 GPa (Michalski et al. 2017; Ebert et al. 2018). As we see evidence for

the shock pressure being distributed heterogeneously in the shocked soil samples, we suggest that shocked clay minerals could make up a significant fraction of the amorphous component of the shocked soil. Alternatively, the particular protolith of the shocked soils might have had less clay minerals than the paleosols used here as a comparison.

It should be noted that exact matches of XRD patterns and mineralogies between the four soils should not be expected as there are slight heterogeneities over even the short distances (~5-6 km from west to east ejecta) of the Lonar region before impact. Whereas the unshocked paleosols show evidence of plagioclase, which is likely labradorite, the presence of local unshocked labradorite in the shocked soils cannot be ruled out due to the heterogeneous nature of shock. Petrography of the shocked soils show both shocked regions with melt and maskelynite needles (formerly labradorite) along with regions of comminuted, unmelted fragments of labradorite and augite (Figure 2). The shocked region is the schlieren of the unshocked region.

Geochemistry

Previous works (Son and Koeberl, 2007; Osae et al. 2005; Schulz et al. 2016; Ray et al. 2017) discussed below on Lonar basalts, impact melts, melt spherules, and paleosol geochemistry have shown an increase in silica and potassium in the soils along with a decrease in aluminum as compared to bedrock basalt. Based on these, we created a ternary plot showing the normalized (to 100%) molar abundances of Si+K, Al, and Ca+Na, or a SK-A-CN plot (Figure 6). This differs from the traditional ternary plots that show S-A-CNK or FM-A-CNK to calculate the chemical or mineralogical alteration of basalts such as Chemical Index of Alteration (CIA) or Mineralogical Index of Alteration (MIA) or Index of Laterization (IOL) (Babechuk et al. 2014).

213 Calculation of these three alteration indexes (CIA, MIA, IOL) are shown for the three shocked
214 soils, average Lonar basalt, and average Lonar paleosol in the supplementary material using
215 methods described by Babechuk (2014) for normalizing moles from geochemical abundances.
216 The values of CIA, MIA, and IOL for basalts and soils agree with those reported for the
217 alteration of basalts from Babechuk (2014) for normalizing moles from geochemical abundances.
218 Figure 6 shows a ternary plot of SK-A-CN in which the three shocked soils plot in between a
219 cluster of 24 published geochemistries of Lonar basalts and six Lonar paleosols.
220

221 **Texture and Spectroscopy**

222 Figures 7 through 10 show the textural relationships among primary igneous minerals, alteration
223 minerals and amorphous phases in three shocked soils. The textures – primarily showing
224 comminuted, rounded silicates is unlike that of Deccan porphyritic basalt (supplemental figure
225 S2; Kieffer et al. 1976; Wright et al. 2011). The spectral signature of these materials in Figures
226 7, 8, and 9 (marked comminuted basalt) looks like average Deccan basalt because the fine-
227 grained minerals are mixed at the sub-pixel scale. Several larger grains are observed however,
228 these include primary igneous phases such as pyroxene (*e.g*. pigeonite) and shocked plagioclase
229 (*i.e.* maskelynite), which has the spectrum of amorphous material of labradorite composition
230 reflected from a lath-shaped pseudomorph of plagioclase. Clay minerals occur as disseminated
231 aggregates of particles throughout, and also have laminated structures in the soil. Note that the
232 precise clay mineralogy is not accessible using infrared reflectance (or emission) in this spectral
233 range. The clays present in this case appear to be trioctahedral (*e.g*. saponite) based on the
234 position of the Si-O reflectance peak, which is located near 1030 cm^{-1} in this case, but would be
235 located near 1060 cm^{-1} in the case of dioctahedral clay (Michalski et al. 2006). Also note that

trioctahedral clays exhibit very few shock effects, unlike dioctahedral clays (Michalski et al. 2017), unless the phyllosilicates are completely melted. Another TIR spectral end-member, basaltic glass (Wyatt et al. 2001), is also detected in the samples. Silicic glass (Wyatt et al. 2001; Jaret et al. 2015) formed from secondary silica deposition and subsequent shock compression (Jaret et al. 2015) show the heterogeneous nature of the shock in the shocked soils. Regions of vesicularity are represented by where epoxy is now evident in the hyperspectral images. A contact between a basaltic region and pockets of organics with rounded silicate minerals and glasses entrained in the organics is suggested in Figure 10. Supplementary figure S6 shows a small region of the same sample LC09-316 (Figures 9, 10) with much clay and some organics.

Discussion

Several previous works have examined the major, minor, and trace element geochemistry of Lonar basalts by comparing the target Deccan basalt to impact melts and various sizes of impact spherules (Son and Koeberl, 2007; Osae et al. 2005; Schulz et al. 2016; Ray et al. 2017). A few have compared the major element and minor element geochemistries of Deccan/Lonar basalt with those of both the paleosol and ejecta fines using spider diagrams (Misra et al. 2006; Newsom et al. 2007; Newsom et al. 2010). These ejecta fines represent pulverized basalt that became the matrix of the lithic breccia. The works comparing paleosols to bedrock basalt show increased silica and potassium in the soils along with a decrease in aluminum attributed to labradorite feldspar being chemically altered and/or physically eroded away (Newsom et al. 2012; Bose et al. 2013), whereas silica is secondary (Jaret et al. 2015). These major element trends agree with previous works examining both soils derived from and emplaced onto Deccan

basalt, and the alteration of Deccan and other basalts (Nesbitt and Wilson, 1992; Babechuk et al. 2014; Wille et al. 2018).

The geochemistries of Deccan paleosol throughout the Deccan region have been noted as being basaltic and very similar to the underlying Deccan basalt (Bhattacharyya et al. 1993; Widdowson et al. 1997; Salil et al. 1997; Ghosh et al. 2006; Sayyed and Hundekari 2006; Pal et al. 2013; Craig et al. 2017). We also note that the geochemistries of the soils used in this study have an overall basaltic composition. It should be noted that mature soils are relatively easy to identify from their geochemistry because mobile elements become depleted and the soil geochemistry and mineralogy contrasts strongly with local bedrock. Immature soils are the opposite case, where the regolith is more similar to underlying rock. As a general trend, mature soils will be thicker and therefore more voluminous (a greater fraction of underlying bedrock and other sources) than immature soils. We focused on five major elements (Si, K, Al, Ca, Na) to emphasize the slight differences between bedrock Deccan basalt and soils. We suggest our ternary plot shows that the three purported shocked soils have a geochemistry different than fresh Lonar basalt, and roughly along the mixing line between fresh basalt and unshocked paleosol (Figure 6). This suggests these shocked soils may have more of a bedrock component than the paleosols, but have some geochemical characteristics of paleosol such as higher Si and K in addition to the soil textures shown in Figures 2, 3, 4, 7, 8, 9, and 10. The alteration mineralogies of the shocked soils are more similar to the palesols than altered basalt (Figure 5). An amorphous component is identified in the shocked soils (Figure 5A) comparable to M-S4 maskelynite-bearing basalt (Figure 5C) and not seen in paleosols (Figure 5B) or unshocked basalt (Figure 5C). This amorphous feature can be directly compared in XRD patterns when comparing Figures 5A and 5B, or the shocked and unshocked basalts in Figure 5C.

Regolith breccias are common among lunar meteorites (Korotev 2012), and have been recognized among Martian meteorites (Cao et al. 2019). However, shocked soils should not be confused with regolith breccias. Regolith breccias are defined as the products of many impacts (Stöffler et al. 2018), or theoretically as a breccia from one impact into a regolith target that required many impacts to form. A soil must be shocked to be classified as a shocked soil. Soil or shocked soil can be inclusions within a regolith breccia, and perhaps future investigations of martian regolith breccias NWA 7034, its pairs NWA 7475 and NWA 7533 (McCubbin et al. 2016; Santos et al. 2015; Cannon et al. 2015; Wittman et al. 2015) or NWA 8171 or NWA 11220 (Cao et al. 2019) might yield the discovery of pockets of martian soil similar to that proposed to exist as melt veins in martian basalt EET79001 (Schrader et al. 2016). Shocked soil should also not be confused with a recent term "lunar impact glasses" (review by Zellner 2019), which are melt droplets emplaced ballistically. Theoretically, a soil could be the protolith of a melt droplet, though the Moon's uppermost surface is generally described as a regolith (Wilcox et al. 2005).

The rarity of shocked soils at the other ~200 terrestrial impact sites is likely due to several factors. The most apparent reason is that a soil surficial unit generally only makes up a very small percentage of the strata affected by the impact. At Lonar crater, even a thicker accumulation of 1-2 meters of soil development is but a small fraction of total strata, with hundreds of meters up to over half a kilometer of bedrock subjected to the shock wave in a crater with an original radius of 0.8-0.9 kilometers. Other factors contributing to the rarity of shocked soil are the small compositional ranges of either granitic or sedimentary target compositions and their ancient ages not contributing to the preservation of impact glasses (such as shocked soil). Regions with granitic-metagranitic "granitoid" compositions or clastic sedimentary rocks and

304 limestones are the most abundant target sequences for a large majority of the ~200 terrestrial
305 impact sites (Schmieder and Kring 2020), but these terrains generally have a paucity of soil
306 development. At impact sites emplaced into these lithologies, local soils resemble the target
307 rocks with little to no alteration, such as pebble-rich sediment from granitic and foliated
308 metamorphic terrains or clastic sediments derived from sedimentary rocks. Their preservation
309 ages are much longer than basalt, and hence the reason they make up the surfaces of continents
310 and a large majority of target rocks at terrestrial impact sites. Essentially, if granitoid or
311 quartzofeldspathic clastic sediments/soils were shocked and found by the field geologist, it
312 would be difficult to recognize them as shocked sediments without a detailed petrographic
313 examination and comparison to their bedrock protoliths. Szokaluk et al. (2019) recently
314 described several reasons why impact sites into consolidated sediments (with no local bedrock)
315 are also rare on Earth and are not preserved for long periods of time. For similar reasons,
316 shocked soils are not preserved as well. Whereas impact melts are found in several terrestrial
317 impact craters as inner crater impact melt pools (review by Dressler and Reimold 1990), intact
318 impact melt-bearing suevite breccias are only found in the ejecta blankets of a handful of the
319 younger impact sites - Ries, Meteor Crater, and Lonar crater. Lonar is one of the youngest of the
320 ~200 terrestrial impact sites (Schmieder and Kring 2020). The mafic target rock, before impact,
321 alters to a soil that can be geochemically, mineralogically, and texturally identified as being
322 unlike the original bedrock basalt that altered to it. This likely would not be true for granitic or
323 clastic sedimentary targets.

324 The discovery of shocked soil is the first of its kind. There are reports of loess (a fine-grained
325 windblown sedimentary deposit) melted to glass in the Pampas region and other regions of
326 Argentina (Schultz et al. 2004; Schultz et al. 2014). However, it has been suggested that these

are fulgerites or the result of fires due to the high frequency of impacts necessary to generate multiple layers of impactites over a short time scale (Chen et al. 2017; Melosh, 2017). Conversely, Howard et al. (2013) discovered organic biomarkers in impact melt, but the protolith was rock and not soil.

Shocked soil is likely not rare on basaltic surfaces with many impact craters and an atmosphere, such as Mars, but is on Earth due to a lack of impact craters into basaltic targets, the aforementioned poor preservation of glassy impactites, and the difficulties with identifying a shocked soil from the majority of terrestrial ejecta blankets. The rarity is shown on Table 12 of Stöffler's (2018) Classification system RE (for "regolith") as the sediment type for unconsolidated sediments of basaltic minerals plagioclase, pyroxene, and olivine is listed as "None", as shocked mafic sediments had not been located in the terrestrial record. The samples described in this paper represent the first examples of shocked unconsolidated basaltic minerals. We suggest these samples be labelled or classified as shocked soils with the evidence presented here that the protolith was soil and not bedrock or sediments. This paper's title alludes to the rarity on Earth (in the sample collections of field geologists) whereas likely more abundant on Mars.

Conclusions

The microscopic texture of the three samples reported here (in Figure 1) showing comminuted basaltic minerals with shock features (Figures 2, 3, 7-10) suggests these samples are shocked soils. Unshocked remnants of soil within the shocked soils (Figures 2, 3 and 4) agree with this interpretation, as does the mineralogy (Figures 5, 7-10) and major element geochemistry (Figure

6). These shocked soils likely have a complicated geologic history, from volcanism to alteration and diagenesis and finally to being shocked to become clasts in an impact melt-bearing breccia unit.

The shocked soils are examples of the complicated nature of impactites that can be expected from planetary surfaces in which soil development occurs. Whereas progressive soil formation will overprint and potentially destroy records of earlier climate, the lithification of a paleosol during impact represents a valuable snapshot of a well-constrained moment in time. These samples represent excellent candidates for sample collection from sample return missions that are unmanned or manned for their information on climatic and geologic conditions for which the soil was created. Further, melted or highly-shocked clasts in them might provide information on the age of the impact event that resulted in the soil being incorporated into the impact breccia. If unshocked remnants exist, whether monomineralic or a rock lithology, then the age of the target rock before impact could be dated and/or constraints on the timing of soil development may be estimated. All of these investigations would benefit the determination of the geologic history of the target rock, the soil development, and the impact event, which are all generally goals of any landed mission.

373

374

375

376 OPEN RESEARCH

377 Data Availability Statement: All data acquired for samples discussed are made publicly

378 available within figures of the paper and in supplementary material.

379

380

381 Supplementary material

382 Supplemental Figure S1 describes the field context of the eastern ejecta blanket of Lonar crater

383 from which the three shocked soils were found. Examples of the petrography of Deccan basalt

384 and M-S4 maskelynite-bearing shocked basalt are shown as supplemental figure S2 to compare

385 to the petrography of shocked and unshocked soils in Figures 2 and 3. Table S3 lists the

386 analyses performed in each figure for the three shocked soils. All geochemical calculations used

387 for Figure 6, including those for all Alteration Indexes derived from molar abundances per

388 Babechuk et al. 2014, can be found as a supplemental .xls file S4. Supplemental figure S5 shows

389 PPL and CPL images of the context of the smaller PPL image in Figure 3E. Supplemental figure

390 S6 shows a smaller clay-rich region with organics in the same sample as Figures 9 and 10.

391

392

393

394 Acknowledgements

395 The authors thank Christopher Hamann for insightful reviews that helped to improve earlier
396 versions of the manuscript. SPW thanks the Department of Forest, Buldana district,
397 Maharashtra, for fieldwork permission. Horton Newsom is thanked for insightful discussions on
398 geochemistry, soil development, and Lonar. SPW thanks Ananda Dube (2010) and Danny
399 Milton (2016) for reminiscing in the field at Lonar and for their nice compliments on SPW's
400 field mapping efforts. Eve Berger and JSC ARES are thanked for assistance on and time on the
401 SEM, respectively. Paul Niles is thanked for his assistance at JSC. The authors thank Adam Liu
402 Jiacheng for his helpful assistance with XRD analyses. Loyc Vanderkluysen and Saumitra Misra
403 assisted SPW with understanding Deccan basalt geochemistry. Stan Mertzman and his lab
404 handled the XRF measurements. Grady Daub helped with sample prep. Anand Mishra assisted
405 SPW during fieldwork. SPW has possession of all samples discussed in this paper. Fieldwork
406 was funded by NASA grant NNX14AP52G. JRM was supported by University of Hong Kong
407 Seed Grant number 201810159005.

408

409

410

411 # References

412

413 Babechuk M.G., Widdowson M., and B.S. Kamber B.S. 2014. Quantifying chemical weathering
414 intensity and trace element release from two contrasting basalt profiles, Deccan Traps, India.
415 *Chemical Geology* **363**: 56-75. doi: 10.1016/j.chemgeo.2013.10.027

416

417 Bhattacharyya T., Pal D.K., and Deshpande S.B. 1993. Genesis and transformation of minerals
418 in the formation of red (Alfisols) and black (Inceptisols and Vertisols) soils on Deccan basalt in
419 the Western Ghats, India. *European Journal of Soil* doi: 10.1111/j.1365-2389.1993.tb00442.x

420

421 Bose T., Misra S., Chakraborty S., and Reddy K. 2013. Gamma (γ)-ray activity as a tool for
422 identification of hidden ejecta deposits around impact crater on basaltic targets: Example from
423 Lonar Crater, India. *Earth, Moon and Planets* **111**, doi: 10.1007/s11038-013-9422-6.

424

425 Cannon C.M., Mustard J.F., and Agee C.B. 2015. Evidence for a widespread basaltic breccia
426 component in the martian low-albedo regions from the reflectance spectrum of Northwest Africa
427 7034. *Icarus* **252**: 150-153. doi: 10.1016/j.icarus.2015.01.016

428

Cao F., Flemming R., Izawa M., and Moser, D. 2019. Determination of mineral deformation in Martian regolith breccias using in situ micro x-ray diffraction and raman spectroscopy. *Geol Soc America Annual Meeting*, 240-5.

Chen J., Elmi C., Goldsby D.L, and Gieré R. 2017. Generation of shock lamellae and melting in rocks by lightning-induced shock waves and electrical heating. *Geophys. Res. Lett*.**44**: doi:10.1002/2017GL073843

Craig P., Chevrier V., Sayyed M.R.G., and Islam R. 2017. Spectral analysis of Deccan intrabasaltic bole beds: implications for the formation and alteration of phyllosilicates on Mars. *Planetary and Space Sciences* **135**: 55-63. doi: 10.1016/j.pss.2016.11.008

Dressler B.O. and Reimold W.U. 2001. Terrestrial impact melts and glasses, *Earth Science Reviews* **56**: 205-284, doi: 10.1016/S0012-8252(01)00064-2

Ebert M., Kowitz A., Schmitt R.T., Reimold W.U., Mansfield U., and Langenhorst F. 2018, Localized shock-induced melting of sandstone at low shock pressures (<17.5 GPa): An experimental study. *Meteoritics and Planetary Science* **53**: 1633–1643, doi: 10.1111/maps.12948

Fudali R.F., Milton D.J., Fredriksson K, and Dube A. 1980. Morphology of Lonar crater, India: Comparison and implications. *The Moon and Planets* **23**: 493-515. doi: 10.1007/BF00897591

Ghosh P., Sayeed M.R.G., Islam R., and Hundekari S.M. 2006. Inter-basaltic clay (bole bed) horizons from Deccan traps of India: Implications for palaeo-weathering and palaeo-climate during Deccan volcanism. *Palaeogeography, Palaeoclimatology, Palaeoecology* **242(1-2)**: 90-109. doi: 10.1016/j.palaeo.2006.05.018

Howard K.T., Bailey, M.J., Berhanu D., Bland P.A., Cressey G., Howard L.E., Jeynes C., Matthewman R., Martins Z., Sephton M.A., Stolojan V., and Verchovsky S. 2013. Biomass preservation in impact melt ejecta. *Nature Geosci*, **6**: 1018–1022. doi:10.1038/ngeo1996

Jay A. E. and Widdowson M. (2008) Stratigraphy, structure and volcanology of the SE Deccan continental flood basalt province: implications for eruptive extent and volumes. *Journal of the Geological Society* **165(1)**: 177-188. doi: 10.1144/0016-76492006-062

Jaret, S.J., Phillips B.L., King Jr D.T., Glotch T.D., Rahman Z, and Wright S.P. 2017. An unusual occurrence of coesite at the Lonar crater, India. *Meteoritics and Planetary Science*, pp 1-17. doi: 10.1111/maps.12745

Jourdan F., Moynier, F., Koeberl, C., Eroglu S. 2011. 40Ar/39Ar age of the Lonar crater and consequence for the geochronology of planetary impacts. *Geology*, **39**: 671–674. doi: 10.1130/G31888.1

Kieffer S.W., Schaal R.B., Gibbons R., Hörz F., Milton D.J., and Dube A. 1976. Shocked basalt from Lonar impact crater, India, and experimental analogues. *Proc. Lunar Planet. Sci. Conf. 7th*: 1391–1412.

Korotev R.L. 2012. Lunar meteorites from Oman. *Meteoritics and Planetary Science* **47(8)**: 1365-1402., doi: 10.1111/j.1945-5100.2012.01393.x

McCubbin F.M., Boyce J.W., Szabó T., Santos A.R., Tartèse R., Domokos G., Vazquez J., Keller L.P., Moser D.E., Jerolmack D.J., Shearer C.K., Muttik N., Steele A., Rahman Z., Anand M., Delhaye T., Agee C.B. 2016. Geologic history of martian regolith breccia Northwest Africa 7034: Evidence for hydrothermal activity and lithologic diversity in the martian crust. *Journal of Geophysical Research* **121(10)**: 2120-2149. doi:

Maloof A. C., Stewart S.T., Weiss B.P., Soule S.A., Swanson-Hysell N.A., Louzada K.L., Garrick-Bethell I., and Poussart P.M. 2010. Geology of Lonar crater, India. *Geological Society of America Bulletin* **122**: 109–126. doi: 10.1130/B26474.1

Melosh H.J. 2017. Impact geologists, beware! *Geophysical Research Letters* **44**: 8873-8874. doi: 10.1002/2017GL074840

Michalski J.R., Kraft M.D., Sharp T.G., Williams L.B., and Christensen P.R. 2006. Emission spectroscopy of clay minerals and evidence for poorly crystalline aluminosilicates on Mars from Thermal Emission Spectrometer data. *Journal of Geophysical Research: Planets* **111**, doi:10.1029/2005JE002438

Michalski J. R., Glotch T.D., Friedlander L.R., Dyar M.D., Bish D.L, Sharp T.G., and Carter J. 2017. Shock metamorphism of clay minerals on Mars by meteor impact. *Geophys. Res. Lett*. **44**: 6562–6569. doi:10.1002/2017GL073423

Misra S., Bose T., Newsom H.E., and Sengupta D. 2006. Geochemistry of impact ejecta from Lonar crater, India – more clues to crater evolution. *37th Lunar and Planetary Science Conference*, #2123.

Nagelschmidt G., Desai A.D., and Muir A. 1940. The minerals in the clay fractions of a black cotton soil and a red earth from Hyderabad, Deccan State, India. *The Journal of Agricultural Science* 30: 639-653. doi: 10.1017/S0021859600048279

Nesbitt H.W. and Wilson R.E. 1992. Recent chemical weathering of basalts. *American Journal of Science* **292**: 740-777. doi: 10.2475/ajs.292.10.740

Nesbitt H.W. and Young G.M. 1989. Formation and diagenesis of weathering profiles, *The*

Journal of Geology 97: 129-147. doi: 10.1086/629290

Newsom H.E., Misra S., and Nelson M.J. 2007. Aqueous alteration of the proximal and distal ejecta blanket at Lonar crater, India. *38th Lunar and Planetary Science Conference* #2056.

Newsom H.E., Misra, S., Wright S.P., and Muttik N. 2010. Contrasting alteration and enrichment of mobile elements during weathering of basaltic ejecta and ancient soils at Lonar crater, India. *41st Lunar and Planetary Science Conference* #2210.

Newsom H.E., Wright S.P., Misra S., and Hagerty J.J. 2013. Comparison of simple impact craters: A case study of Meteor and Lonar craters. In Impact Cratering: Processes and products, editors Osinksi and Pierazzo. Chapter 18. Pages 271-289. doi: 10.1002/9781118447307.ch18

Osae S., Misra S., Koeberl C., Sengupta D., and Ghosh S. 2005. Target rocks, impact-glasses and melt rocks from the Lonar impact crater, India: Morphology, petrography and geochemistry. *Meteoritics & Planetary Science* 40: 1473–1492. doi: 10.1111/j.1945-5100.2005.tb00413.x

Osinski G.R. and Pierazzo E. 2013. Impact cratering: Processes and products. Blackwell Publishing. 336 pages. doi: 10.1002/9781118447307

533 Pal D.K., Wani S.P., and Sahrawat K.L. 2013. Zeolitic soils of the Deccan basalt areas in India:
534 their pedology and edaphology. *Current Science* **105**: 309-318.

535

536 Peng Z.X, Mahoney J.J., Vanderkluysen L., Hooper P.R. 2014. Sr, Nd and Pb isotopic and
537 chemical compositions of central Deccan Traps lavas and relation to southwestern Deccan
538 stratigraphy. *Journal of Asian Earth Sciences* **84**: 83-94. doi: 10.1016/j.jseaes.2013.10.025

539

540 Ray D., Upadhyay D., Misra S., Newsom H.E., and Ghosh S. 2017. New insights on
541 petrography and geochemistry of impactites from the Lonar crater, India. *Meteoritics and*
542 *Planetary Science* **52**: 1577-1599. doi: 10.1111/maps.12881

543

544 Santos A.R., Agee C.B., McCubbin F.M., Shearer C.K., Burger P. V., Tartèse R., Anand M.
545 2015. Petrology of igneous clasts in Northwest Africa 7034: Implications for the petrologic
546 diversity of the martian crust. *Geochimica et Cosmochimica Acta* **157**: 56-85. doi:

547

548 Salil M.S., Shrivastava J.P. and Pattanayak S.K. 1997. Similarities in the mineralogical and
549 geochemical attributes of detrital clays of Maastrichtian Lameta Beds and weathered Deccan
550 basalt, Central India. *Chemical Geology* **136**: 25-32. doi: 10.1016/S0009-2541(96)00128-3

551

552 Sayyed M.R.G. and Hundekari S.M. 2006. Preliminary comparison of ancient bole beds and
553 modern soils developed upon the Deccan volcanic basalts around Pune (India): Potential for

palaeoenvironmental reconstruction. *Quaternary International* **156-157:** 189-199. doi: 10.1016/j.quaint.2006.05.030

Schmieder M. and Kring D.A. 2020. Earth's Impact Events Through Geologic Time: A List of Recommended Ages for Terrestrial Impact Structures and Deposits. *Astrobiology* **20**:1, doi: 10.1089/ast.2019.2085

Schrader C.M., Cohen B.A., Donovan J.J., and Vicenzi E.P. 2016. Ni/S/Cl systematics and the origin of impact-melt glasses in Martian meteorite Elephant Moraine 79001. *Meteoritics and Planetary Science* **51(4):** 663-680. doi: 10.1111/maps.12612

Schultz P. H., Zárate M., Hames, B., Koeberl C., Bunch T., Storzer D., Renne P., and Wittke J. 2004. The Quaternary impact record from the Pampas, Argentina. *Earth Planet. Sci. Lett*. **219**(3–4): 221–238. doi:10.1016/S0012-821X(04)00010-X.

Schultz P.H., Harris R.S., Clemett S.J., Thomas-Keprta K.L., and Zárate M. 2014. Preserved flora and organics in impact melt breccias. *Geology* **42**(6): 515–518. doi: https://doi.org/10.1130/G35343.1

Schulz T., Luguet A., Wegner W., van Acken D., and Koeberl C. 2016. Target rocks, impact glasses, and melt rocks from the Lonar crater, India: Highly siderophile element systematics and

575 Sr-Nd-Os isotopic signatures. *Meteoritics and Planetary Science* **51**: 1323-1339. doi:
576 10.1111/maps.12665

577

578 Shoemaker E.M. 1960. Penetration mechanics of high velocity meteorites, illustrated by Meteor
579 Crater, Arizona. *21st International Geological Congress*, Copenhagen, pages 418-434.

580

581 Son T.H. and Koeberl C. 2007. Chemical variation in Lonar impact glasses and impactites.
582 *GFF* **129:** 11-176. doi: 10.1080/11035890701292161.

583

584 Stewart S.T., Louzada K.L., Maloof A.C., Newsom H.E., Weiss B.P., and Wright S.P. 2005.
585 Field observations of ground-hugging ejecta flow at Lonar crater, India. *Workshop on the Role of*
586 *Volatiles and Atmospheres on Martian Impact Craters,* abstract #3045.

587

588 Stöffler D., Hamann C., and Metzler K. 2018. Shock metamorphism of planetary silicate rocks
589 and sediments: Proposal for an updated classification system. *Meteoritics and Planetary Science*
590 **53**: 5-43. doi: 10.1111/maps.12912

591

592 Szokaluk M., Jagodziński R., Muszyński A., and Szczuciński W. 2019. Geology of the Morasko
593 craters, Poznań, Poland—Small impact craters in unconsolidated sediments. *Meteoritics &*
594 *Planetary Science* **54**(7), pp. 1478-1494. doi: 10.1111/maps.13290

595

596 Vanderkluysen L, Mahoney J.J., Hooper P.R., Sheth H.C., and Ray R. (2011) The feeder system
597 of the Deccan Traps (India): Insights from dike geochemistry. *Journal of Petrology*, 52: 315–
598 343. doi: 10.1093/petrology/egq082

599

600 Wilcox B.B., Robinson M.S., Thomas P.C., and Hawke B.R. 2005. Constraints on the depth
601 and variability of the lunar regolith. *Meteoritics and Planetary Science* 40: 695-710. doi:
602 26 10.1111/j.1945-5100.2005.tb00974.x

603

604 Wille M., Babechuk M.G., Kleinhanns I.C., Stegmaier J., Suhr N., Widdowson M., Kamber B.S.,
605 and Schoenberg R. 2018. Silicon and chromium stable isotopic systematics during basalt
606 weathering and lateritisation: A comparison of variably weathered basalt profiles in the Deccan
607 Traps, India. *Geoderma* **314**: 190-204. doi: 10.1016/j.geoderma.2017.10.051

608

609 Wittman A., Korotev R.L., Joliff B.L., Irving A.J., Moser D.E., Barker I., and Rumble III B.
610 2015. Petrography and composition of Martian regolith breccia meteorite Northwest Africa
611 7475. *Meteoritics and Planetary Science* **50**(2): 326-352, doi: 10.1111/maps.12425

612

613 Wright S.P., Christensen P.R., and Sharp T.G. 2011. Laboratory thermal emission spectroscopy
614 of shocked basalt from Lonar Crater, India, and implications for Mars orbital and sample data.
615 *Journal of Geophysical Research – Planets* **116**(E9), doi: 10.1029/2010JE003785

616

Wyatt M.B., Hamilton V.E., McSween H.Y., Christensen P.R., and Taylor L.A. 2001. Analysis of terrestrial and Martian volcanic compositions using thermal emission spectroscopy: 1. Determination of mineralogy, chemistry, and classification strategies, J. Geophys.Res., **106**(E7), pp 14711 – 14732.

Zellner N.E.B. 2019. Lunar impact glasses: Probing the Moon's surface and constraining its impact history. *Journal of Geophysical Research – Planets*, doi: 10.1029/2019JE006050

FIGURE CAPTIONS

Figure 1. Hand samples of shocked soils. On the left is a cut surface of a maskelynite-bearing basalt (shock stage M-S4) with shocked soil adhered to the bottom and bottom right of the sample. Within the lighter gray shocked soil adhered to the bottom right of the sample, note lighter gray color and small white calcite portions similar to the samples on the right. On the right are cut billets (upper four) and natural sides (lower three) of shocked soils samples LC15-497, LC09-304, and LC09-316 discussed in the text. Note layered white shocked calcite in several samples that we interpret as caliche horizons in the original soil and shown in Figure 2.

Figure 2. Petrography of samples LC09-316 (A-D) and LC09-304 (EF) interpreted to be shocked soils, with plane polarized light (PPL) on the left and the same field of view in cross polarized light (CPL) on the right. Scale bar measuring 500 μm in (EF) applies to all 8 panels; all 8 images are taken with 5X magnification. Sample LC09-316 in AB shows light brown caliche from top to bottom through the center of the top two images, with tiny ~5-10 μm comminuted particles of augite and labradorite (labeled "aug, lab") on the right. The second set of photomicrographs (CD) shows schlieren calcite from the top right to the bottom left of the images. The calcite has high birefringence in CPL in (D). In EF, flowing caliche is shown in sample LC09-304 from the upper left to bottom center (white in CPL) with melted basaltic glass (light brown in PPL and labeled "melt") on the left and a maskelynite needle on the right (labeled "mask" and isotropic in CPL in (F)). In GH, an unshocked paleosol collected from under the Lonar lithic breccia unit shows a similar texture as pockets of comminuted augite and labradorite on the right sides of AB and CD along with examples of caliche layers and pockets that presumably was melted and flowed in the shocked soils shown in the first six panels.

Figure 3. High resolution (20X – 40X) petrographic images of unshocked soil remnants within shocked soil sample LC09-316. All scale bars for A through E are 100 μm while the scale bar for F is 50 μm. (A) in PPL and (B) in CPL show a remnant paleosol with desiccation crack features at 20X magnification amidst glass around it. The background glass is blurry whereas the unshocked soil remnant is focused under these higher resolutions. (CD) shows the 4 clumps of unshocked soil (darker in PPL) that are shown in the context BSE image in Figure 4A and

focused BSE images Figures 4C and 4D. Figure 3E (only PPL) shows another set of remnant relicts of soil, but with melted glassy edges. Supplemental figure S5 shows the context image of Figure 3E at 5X magnification in both PPL and CPL, and compared to other basaltic end members besides soil in supplemental figure S2. (F) in PPL shows a circular unshocked soil remnant with desiccation crack features at 40X magnification. Scale bar for F measures 50 μm.

Figure 4. Backscattered electron (BSE) images of shocked soil LC09-316 (in A, C, and D) and unshocked Deccan soil (B) showing nearly the same area as the petrography shown in Figure 3CD. The magnification on the image and the measure of each scale bar is noted under each of the four panels. In all four panels, bright white are oxides, the darkest grays are glasses or crystals of labradorite composition, and the lightest grays are augites. In A, note three teardrop-shaped regions across the middle of the BSE image with desiccation cracks within the clasts, but flow textures outside the three clasts. We interpret these as unshocked soil remnants within the shocked soil, suggesting the protolith of the impactite was soil. A fourth similarly-textured region is a smaller triangle-shaped region just below the region in between the middle and rightmost circular area with desiccation cracks, but does not exhibit desiccation cracks. Panel C shows a higher resolution of leftmost two (at 300X resolution) and panel D shows the rightmost clast (at 650X resolution). There is a boundary of melted/shocked and unmelted around the unshocked soil remnants. The desiccation textural features of these regions match the texture of unshocked Deccan soil (in panel B) shown at the same resolution (120X) as the shocked soil in panel A.

Figure 5. XRD patterns of several Lonar samples for comparison and mineralogic analyses. An amorphous component and alteration minerals are found in the shocked soils (A). Similar alteration minerals, but no amorphous component, are found in the unshocked paleosols (B). (C) shows a comparison of unshocked and shocked bedrock basalt to note the added amorphous component (maskelynite) of shocked basalt not found in unshocked basalt (also C) or paleosols (B).

Figure 6. The lower right portion of a A-CN-SK geochemical plot of basalts and soils. 19 Lonar fresh basalts (from Osae et al. 2005 and described by Ray et al. (2017) as the basis of "avg Lonar basalt") are shown as blue circles, another 5 Lonar fresh basalts from Peng et al. (2014) shown as orange circles, three shocked soils as black triangles, average Lonar paleosol (n=6 from Misra et al. 2006) as a gray circle, and the geochemistry of one paleosol in green (from Figures 2GH and 3B) collected with the same methods as the three shocked soils. The major element geochemistry of all shown here and various chemical alteration indexes (Babechuk et al. 2014) are shown in the supplemental material. A mixing line between the cluster of 24 fresh basalts and the gray or green paleosol point would be identical to the mixing line suggested by Newsom et al. 2010.

Figure 7. A micro-infrared image of shocked soil sample LC09-497 displays principal components 4, 3 and 2 as RGB respectively. Image measures 3 mm by 10 mm. In this band combination, diaplectic maskelynite (marked "M") and an example of flowing labradorite glass

both appear blue in the image, calcite (Cal) appears white, clay minerals appear purple-indigo, comminuted, fine grained basaltic materials appear green to green-yellow-brown (marked "Bas"). The spectra extracted from the reflectance image are color coded to the PCA image with the exception of calcite, which appears white in the image but is displayed as a black spectrum. "E" labels the epoxy that is a proxy for the vesicularity of the original sample before adhering it to a thin section.

Figure 8. A micro-infrared image of shocked soil sample LC09-304 displays principal components 4, 3 and 2 as RGB respectively. Image measures 4 mm by 10 mm. In this band combination, pigeonite (marked "Pyx") appears red in the image, amorphous silica (Si) appears bright green, clay minerals appear indigo, comminuted, fine grained basaltic materials appear yellow-brown (marked "Bas"). The spectra extracted from the reflectance image are color coded to the PCA image. "E" labels the epoxy that is a proxy for the vesicularity of the original sample before adhering it to a thin section.

Figure 9. Two micro-infrared images of one sample LC09-316 showing rounded augites, pigeonites, and needles of maskelynite or glass of plagioclase composition after shock compression converted the original labradorite to a glass. Silica glass is also apparent throughout the sample. Whereas light blue is plagioclase glass, dark blue is epoxy and not shown on the spectral plot.

Figure 10. A 6 mm by 6 mm micro-infrared reflectance image of sample LC09-316 showing the likely contact between organics and silicates in the shocked soil. Rather than PCA's shown in

Figures 7, 8, 9, Figure 10 displays bands 110-97-86 (1079 cm-1, 1022 cm-1, 979 cm-1) in red, green, and blue, respectively. Whereas most dark black regions are epoxy (not shown in the spectral plot) indicating vesicularity as small circles within larger black pockets, isolated black pixels at the top left and bottom right have a flat spectrum with little spectral character and low reflectance. Whereas these could be oxides or sulfides, the previously-published mineralogies of Deccan soil (see text) and petrography (Figures 2 and 3) suggest these are organics with no discerning spectral features such as the lowest gray-black spectrum shown in the spectral plot. All spectra in the spectral plot are color-coded to the RGB image save for white augite in the image is displayed as a black spectrum in the spectral plot. Tiny bits of pigeonite (pink), maskelynite (red), Si glass (yellow), while one large clump and many small bits of clay (cyan) can be seen. Rare pixels of Si-K glass (blue) can be see above and to the right of the largest cyan clay region. Comminuted basalt in forest green is not shown in the spectral plot.

SUPPLEMENTAL FIGURE AND TABLE CAPTIONS

Figure S1. The names of GPS points from several field seasons are plotted on a subset of a QuickBird image of Lonar crater from Maloof et al. (2010) of the eastern ejecta blanket. North is up. The eastern rim is on the left of this subset, and thus the crater interior is west of this proximal eastern ejecta blanket. The three shocked soils described in Wright and Michalski (2024) were found in the eastern ejecta blanket at and nearby GPS point labelled “EES” for east ejecta suevite. The coordinates are 19.975° N, 76.518° E. Examples of the east ejecta suevite outcrops are shown as shocked soil samples LC09-304 and LC09-316 were both collected next

to a large clast LC09-EES-315 (top and middle field photos). A suevite outcrop showing M-S7 impact melt as a dark black glass clast is also shown (bottom field photo). Rock hammer pick points to the crater rim or crater center in all pictures.

Figure S2. The petrography of Deccan bedrock basalt in plain polarized light (left) and cross polarized light (right) can be compared to the petrography of shocked soils in Figures 2, 3, and S5. Scale bar in lower right corner of top two images measures 500 μm for all four images. Shocked soil and unshocked paleosol (Figures 2 and 3 in *Wright and Michalski* 2024) contain organics, calcite, clays, and tiny bits of comminuted, rounded augite and labradorite and not the larger euhedral grains of augite and labradorite seen here. Note that twinned labradorite (in CPL) is converted to diaplectic maskelynite in the shock stage M-S4 shocked basalt in the lower two panels, whereas augites are fractured. The grain sizes of the silicate minerals are not comminuted and rounded by shock. Secondary hematite is seen as red in the M-S4 shocked basalt in the lower images.

Table S3. The analyses performed for three shocked soils and three paleosols and the corresponding figure in Wright and Michalski (2024) are shown.

sample	sample texture	petrography, BSE images	XRD mineralogy	geochemistry	μFTIR
LC09-304	1	2	5	6	8

LC09-316	1	2, 3, 4, S5	5	6	9, 10, S5
LC15-497	1			6	7
LC15-PS-456			5		
LC15-PS-460		4	5	6	
LC15-PS-287		2			

Figure S4. (entire 24 kilobyte .xls file is a shared Supplemental File and not a table)

Figure S4. The geochemical data used for a ternary plot in Figure 6. The XRF geochemistry data was converted to moles using the methods described in Babechuk et al. (2014) to compare the abundances of Si, K, Al, Ca, Na for 24 bedrock Deccan basalts (Osae et al. 2005; Peng et al. 2014; Ray et al. 2017), seven Deccan palesols (Misra et al. 2006; Ray et al. 2017), and three shocked soils.

Figure S5. High resolution petrographic images, in plain polarized and cross polarized light, of the context of the field of view seen in Figure 3E of Wright and Michalski (2024). The red box denotes the approximate area of the entirety of Figure 3E. All dark circles and shapes are remnants of unshocked soil within glass that used to be unshocked soil, but is now shocked soil.

794 The scale bar in the lower right corner measures 500 μm. Figure 3E shows melting on the edges
795 of these unshocked soil remnants.
796
797
798
799 Figure S6. Bands 4, 3, and 2 of a principle component analyses are displayed as red, green, and
800 blue, respectively, of a 2.9 mm by 1.8 mm region of shocked soil LC09-316. Two clays are
801 shown as red and green in the PCA image with white bits of basalt in the image being
802 represented as a black spectrum in the spectral plot. In addition, in the lower right of the image,
803 a brownish spectrally featureless material with a small amount of clay (note same 1030 cm-1
804 peak as the clay in the red spectrum) is interpreted to be organics in the shocked soil. The clay in
805 the green pixels of the image are spectrally similar to the red pixels, and thus only the red clay
806 end-member is shown in the spectral plot with basalt (black spectrum, white pixels) and organics
807 (brown).
808

Figure 1.

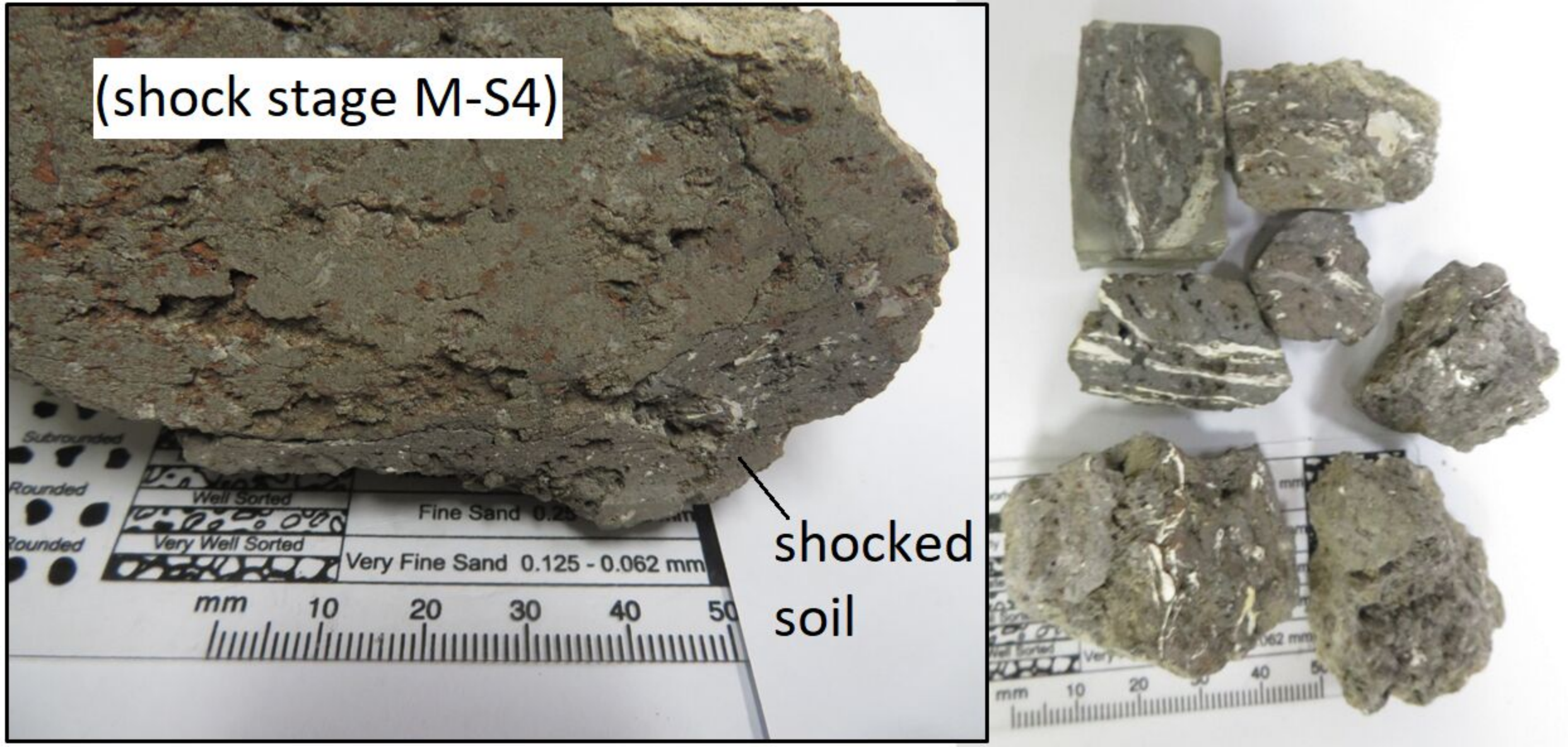
(shock stage M-S4)
shocked soil
Subrounded
Rounded
Rounded
Well Sorted
Very Well Sorted
Fine Sand
Very Fine Sand 0.125 - 0.062 mm
mm
10
20
30
40
50

Figure 2.

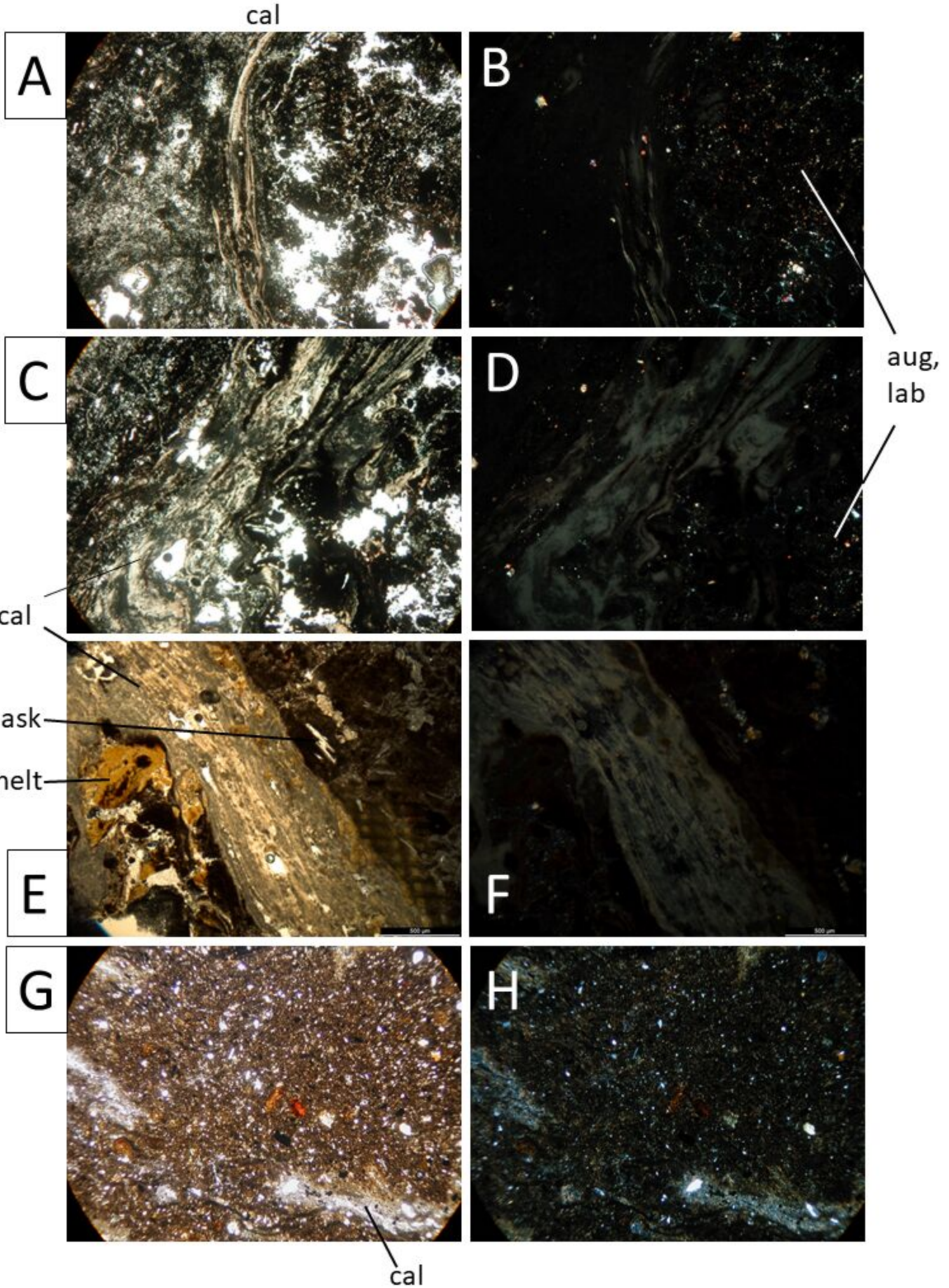
cal
A
B
aug,
lab
C
D
cal
mask
melt
E
F
G
H
cal

Figure 3.

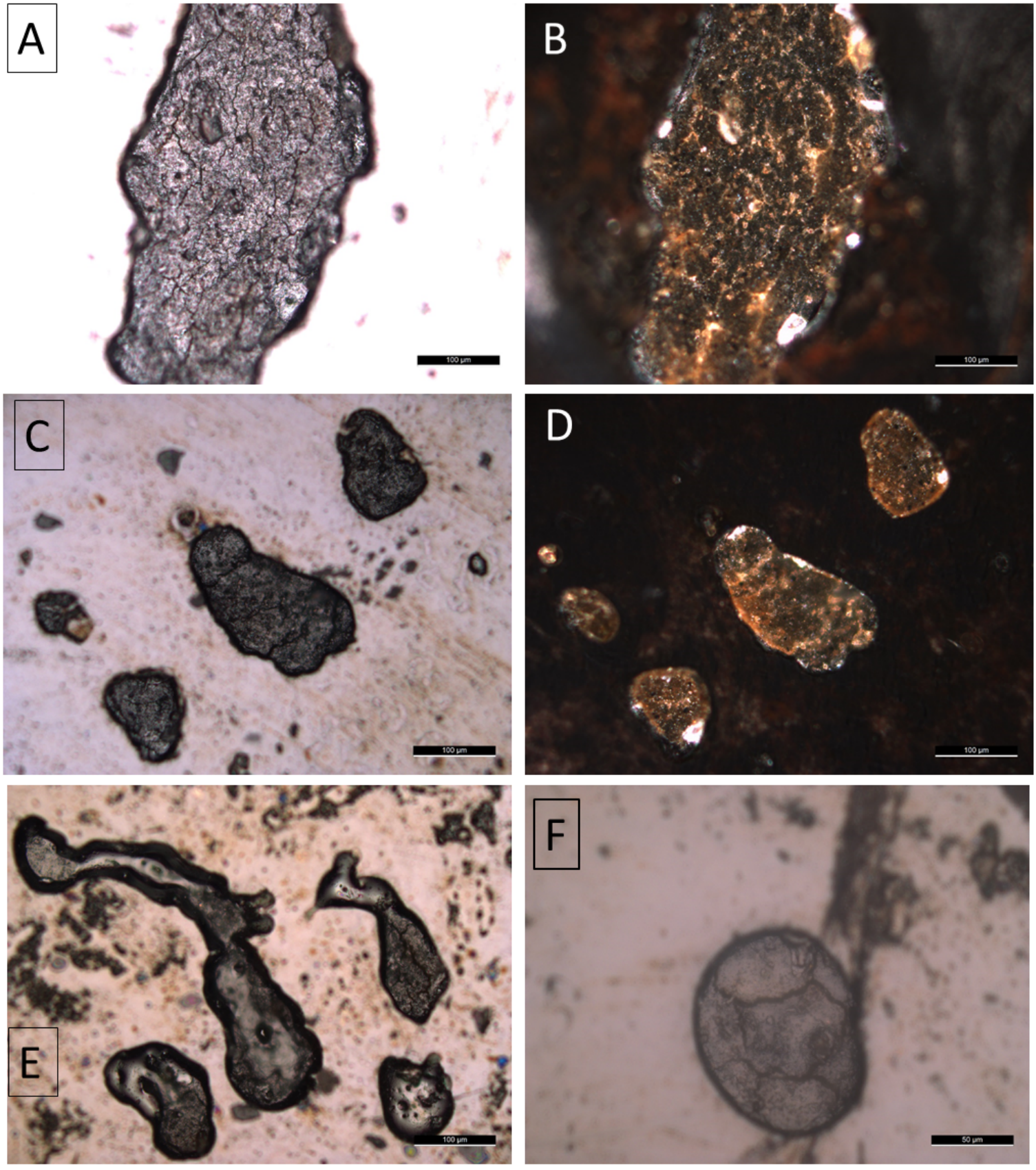
A
100 µm
B
100 µm
C
100 µm
D
100 µm
E
100 µm
F
50 µm

Figure 4.

Figure 3.

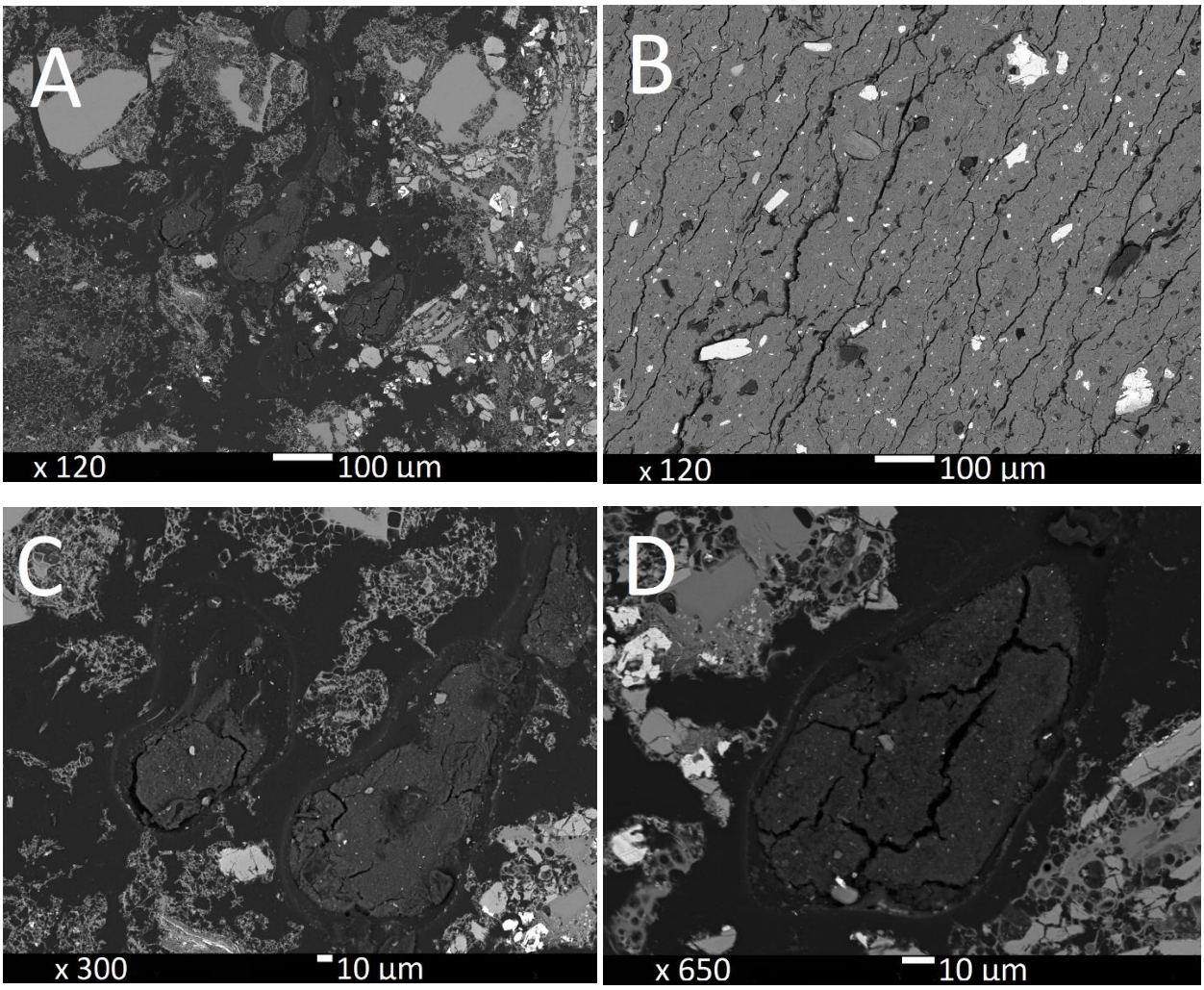

Figure 5.

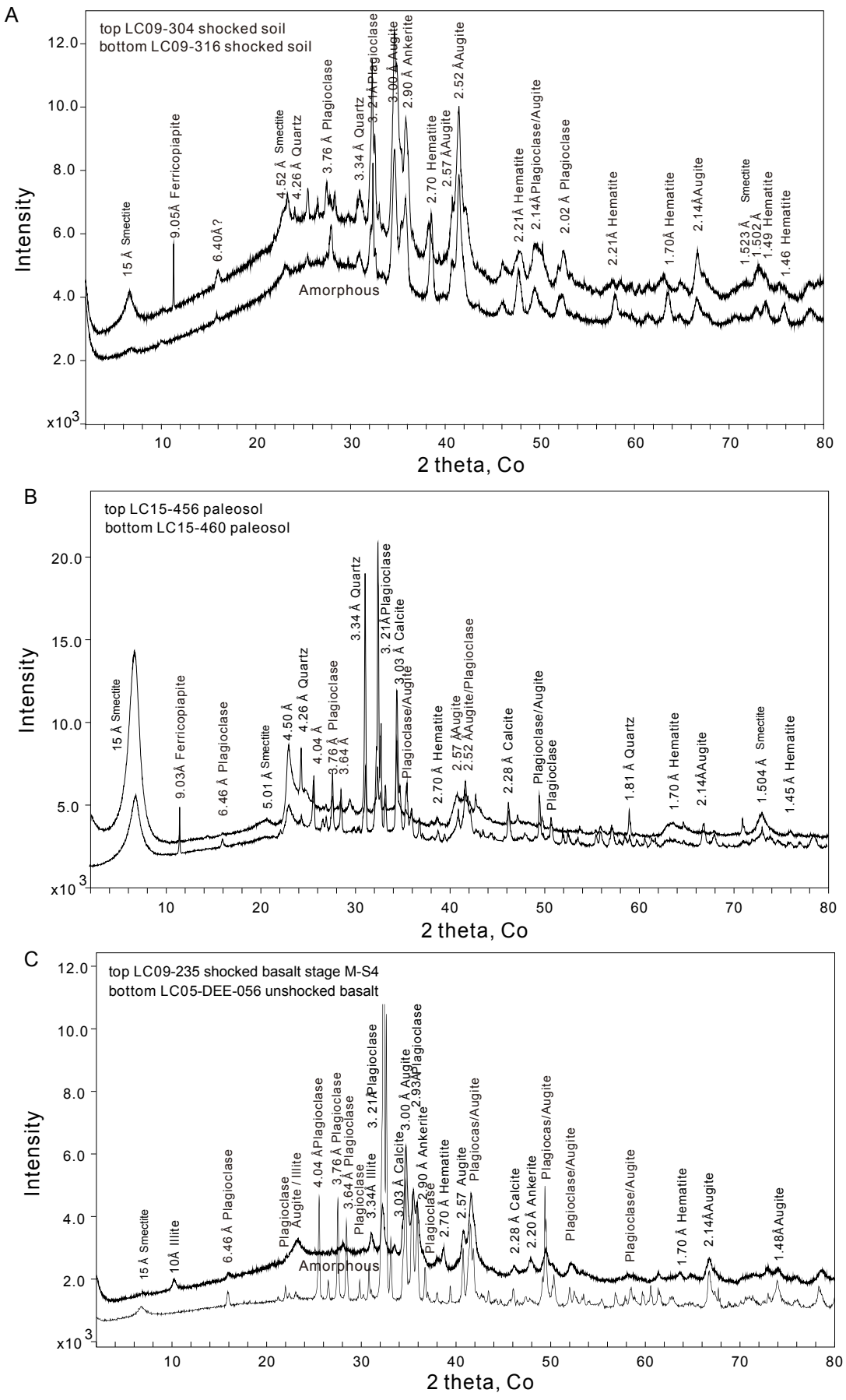
A
top LC09-304 shocked soil
bottom LC09-316 shocked soil
Intensity
x10 3
2 theta, Co
15 Å Smectite
9.05Å Ferricopiapite
6.40Å ?
4.52 Å Smectite
4.26 Å Quartz
3.76 Å Plagioclase
3.34 Å Quartz
3. 21Å Plagioclase
3.00 Å Augite
2.90 Å Ankerite
2.70 Hematite
2.57 ÅAugite
2.52 ÅAugite
2.21Å Hematite
2.14ÅPlagioclase/Augite
2.02 Å Plagioclase
2.21Å Hematite
1.70Å Hematite
2.14ÅAugite
1.523 Å Smectite
1.502 Å
1.49 Hematite
1.46 Hematite
Amorphous
B
top LC15-456 paleosol
bottom LC15-460 paleosol
Intensity
x10 3
2 theta, Co
15 Å Smectite
9.03Å Ferricopiapite
6.46 Å Plagioclase
5.01 Å Smectite
4.50 Å
4.26 Å Quartz
4.04 Å
3.76 Å Plagioclase
3.64 Å
3.34 Å Quartz
3. 21Å Plagioclase
3.03 Å Calcite
Plagioclase/Augite
2.70 Å Hematite
2.57 ÅAugite
2.52 ÅAugite/Plagioclase
2.28 Å Calcite
Plagioclase/Augite
Plagioclase
1.81 Å Quartz
1.70 Å Hematite
2.14ÅAugite
1.504 Å Smectite
1.45 Å Hematite
C
top LC09-235 shocked basalt stage M-S4
bottom LC05-DEE-056 unshocked basalt
Intensity
x10 3
2 theta, Co
15 Å Smectite
10Å Illite
6.46 Å Plagioclase
Plagioclase
Augite / Illite
4.04 ÅPlagioclase
3.76 Å Plagioclase
3.64 Å Plagioclase
3.34Å Illite
3. 21Å Plagioclase
3.03 Å Calcite
3.00 Å Augite
2.93Å Plagioclase
2.90 Å Ankerite
Plagioclase
2.70 Å Hematite
2.57 Augite
Plagiocas/Augite
2.28 Å Calcite
2.20 Å Ankerite
Plagiocas/Augite
Plagioclase/Augite
Plagioclase/Augite
1.70 Å Hematite
2.14ÅAugite
1.48Å Augite
Amorphous

Figure 6.

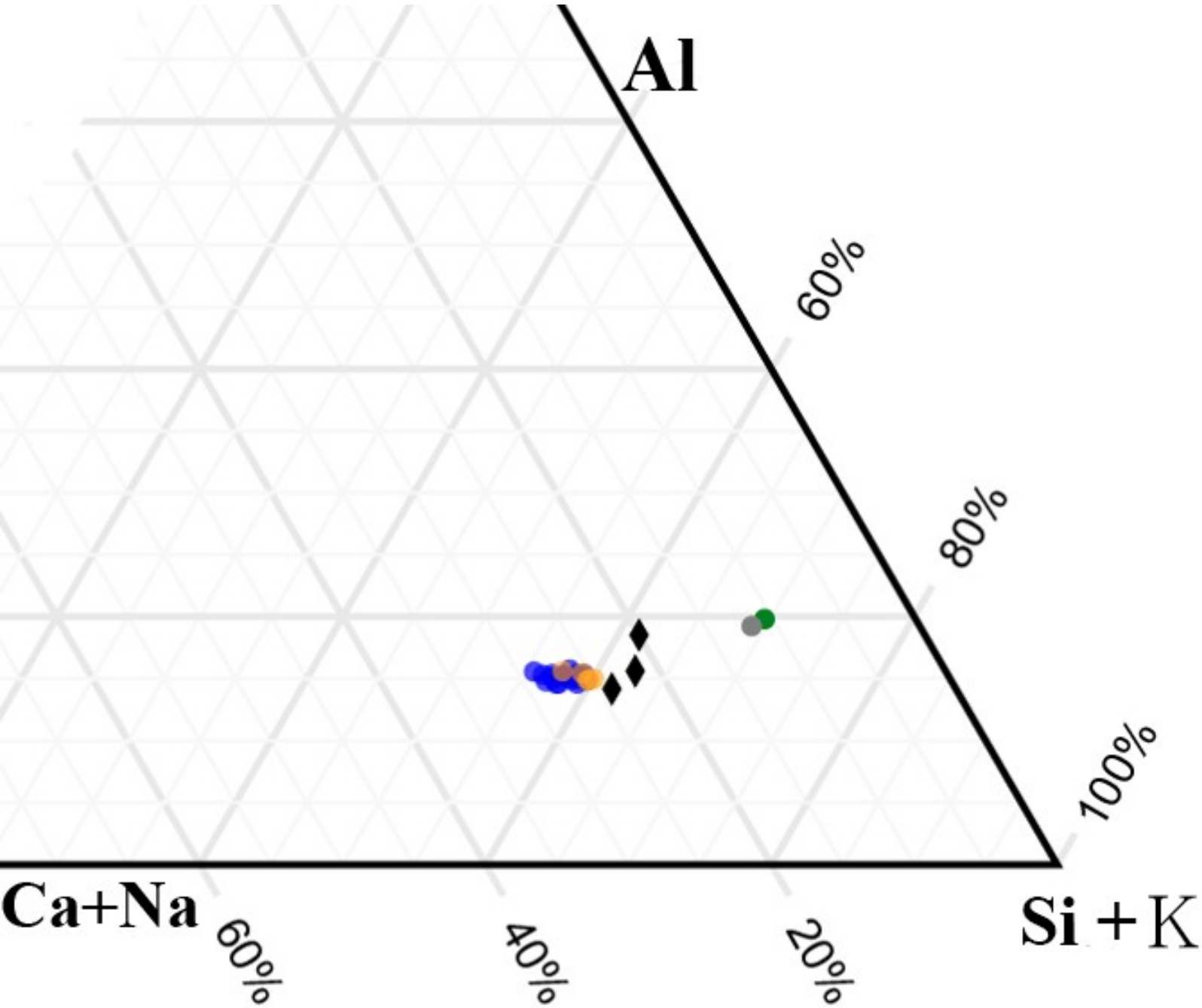
Al
60%
80%
100%
Ca+Na
60%
40%
20%
Si +K

Figure 6 legend.

- 19 Lonar basalts (Osae et al. 2005; Ray et al. 2017)
- 5 Lonar basalts (Peng et al. 2014)
- ♦ 3 shocked soils
- avg Lonar paleosol (n=6) (Misra et al. 2006)
- 1 Lonar paleosol

Figure 7.

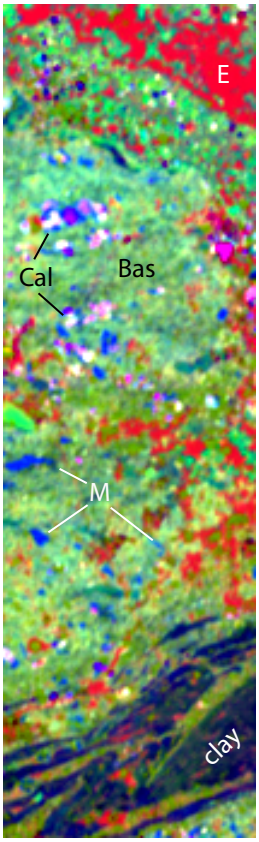
E
Cal
Bas
M
clay

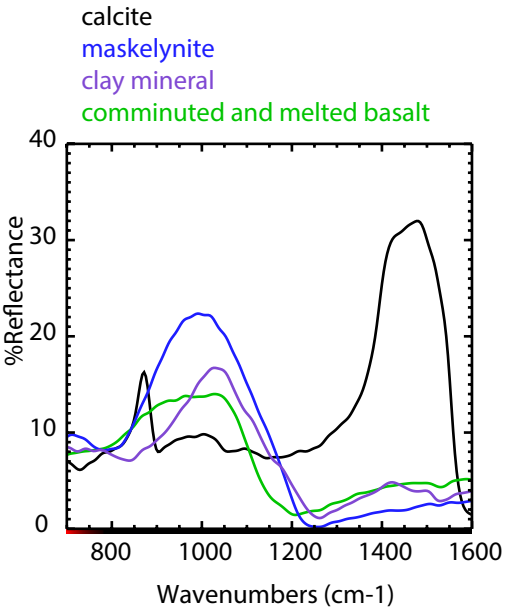
calcite
maskelynite
clay mineral
comminuted and melted basalt
40
30
20
10
0
%Reflectance
800
1000
1200
1400
1600
Wavenumbers (cm-1)

Figure 8.

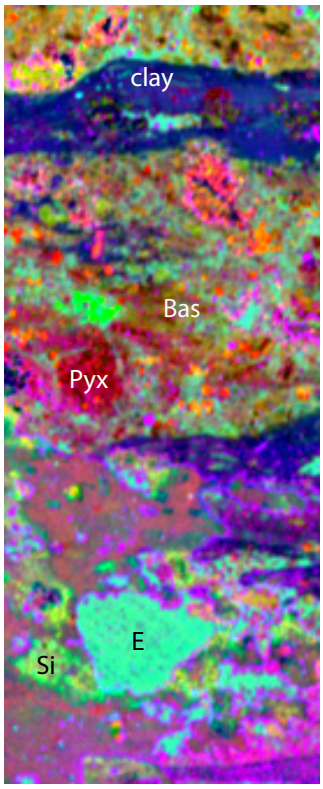

pigeonite
clay mineral
amorphous silica/silica glass
comminuted and melted basalt

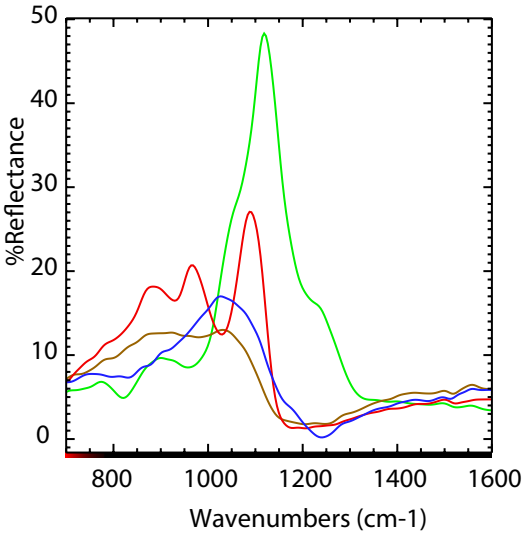

Figure 9.

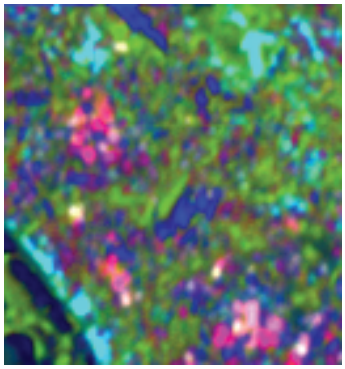

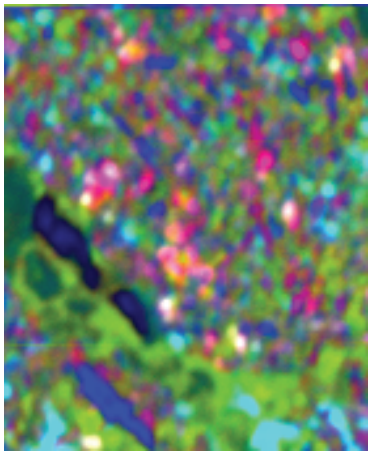

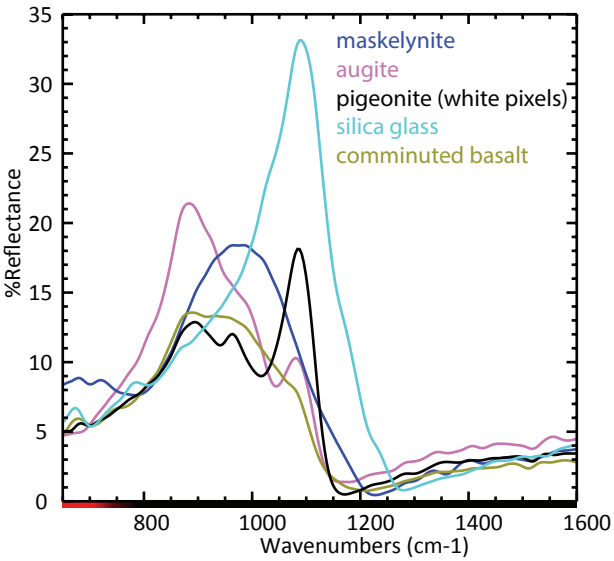
maskelynite
augite
pigeonite (white pixels)
silica glass
comminuted basalt
%Reflectance
Wavenumbers (cm-1)
0
5
10
15
20
25
30
35
800
1000
1200
1400
1600

Figure 10 uFTIR.

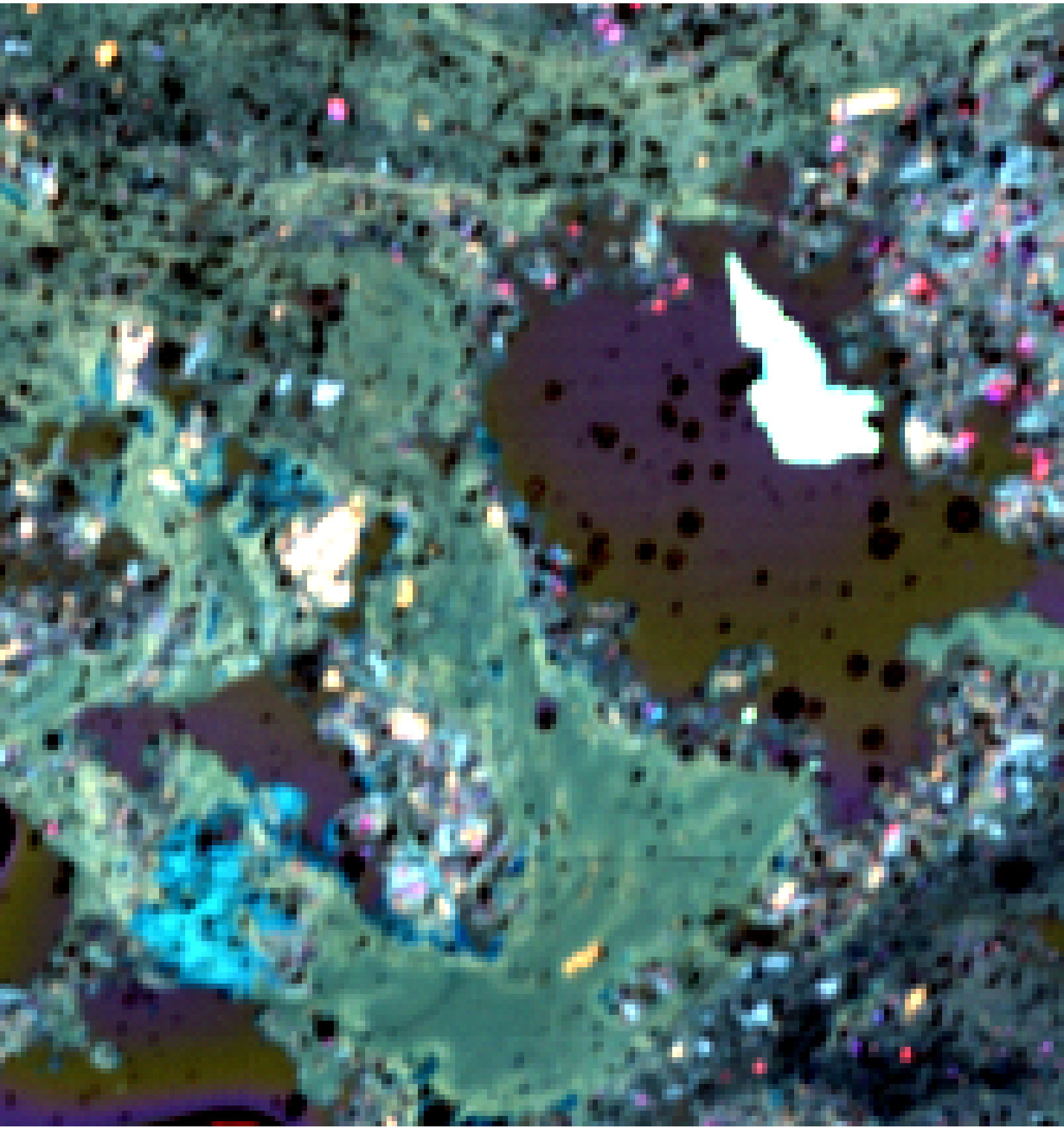

Figure 10 spectral plot.

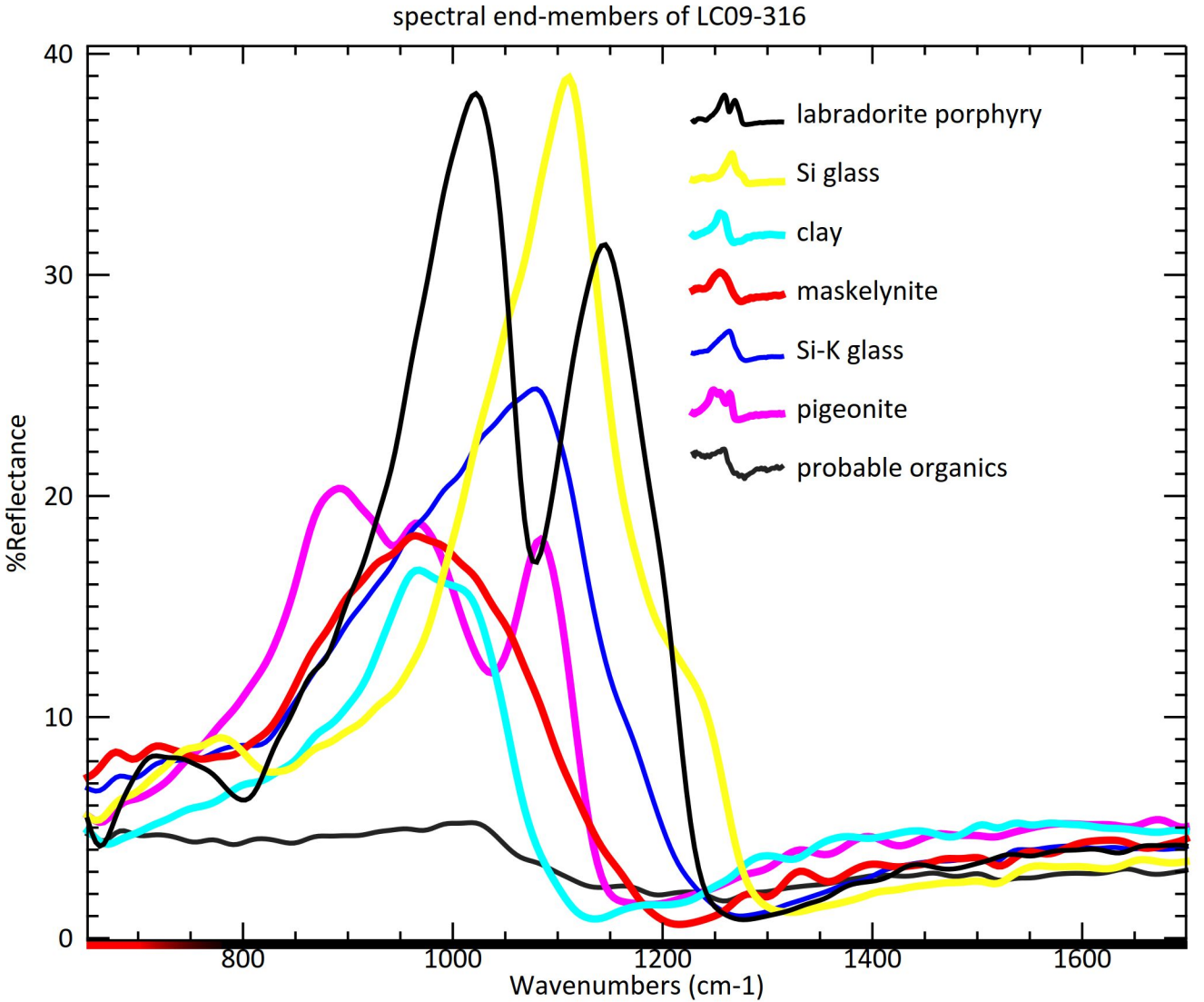
spectral end-members of LC09-316
labradorite porphyry
Si glass
clay
maskelynite
Si-K glass
pigeonite
probable organics
%Reflectance
Wavenumbers (cm-1)
0
10
20
30
40
800
1000
1200
1400
1600